2011 American Control Conference
on O'Farrell Street, San Francisco, CA, USA
June 29 - July 01, 2011

A Feasibility Assessment of Using Ultrasonic Sensor Position Feedback for a Ball-and-Beam Apparatus

Jacob Wieneke and Warren N. White

Abstract—**The process of testing and implementing ultrasonic transducers for ball position feedback on a ball-and-beam apparatus is described. Various ball-and-beam configurations are described as well as the specific configuration used in this work. Details include choices in sensors, hardware, construction, and controller design. The weight symmetry constraint necessitates using two sensors. Information is provided as to how the two sensors are used without creating interference. Measured initial condition and disturbance responses are presented. The conclusions indicate that acoustic sensors can complete a successful ball-and-beam system.**

I. Introduction

THE ball-and-beam device in controls education provides an example of underactuated mechanical systems and examples of LQR and pole placement design. Constructions can vary, but the principles are similar: a ball rolls freely on a beam and the beam angle is changed to control the ball position. Sensors are used to determine the ball location and the beam angle. A controller either stabilizes the ball at a given location or makes the ball track a reference trajectory.

This work explores ultrasonic sensor usage for ball position feedback. The specifics of the device used for this work: physical details, sensor selection, controller design, and system performance are covered and contrasted with other ball-and-beam constructions. Notable in the presentation is information regarding how to use the two symmetrically located sensors so there is no cross sensor interference. A link to a website containing CAD drawings, software downloads, parts list, and images/video is included.

A. Beam Configurations

The ball-and-beam can be constructed many ways. The commonality is a change in beam angle based on a corresponding change in actuator angular position.

1) Fixed-End Beam Construction

Fig. 1 shows a beam end fixed to a rotational joint and the other end is connected to a linkage, allowing beam pitch control. Such a device is commercially available [1].

2) Rotational Beam Interface

Fig. 2 shows how the rotational beam drive allows the motor to change the beam angle by driving a disk to counter-rotate a semicircular disk on the beam. The beam center is fixed. This method of construction was used at MIT for an undergraduate class project [2]. Instead of a disk, it is possible to use a gear system, which reduces slippage [3].

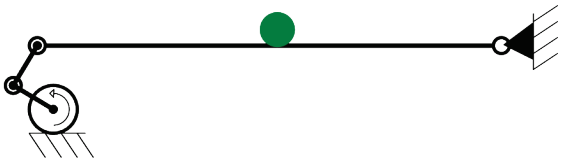

Fig. 1: Fixed-End Beam

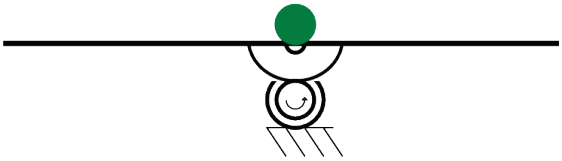

Fig. 2: Rotational Beam Interface

3) Motor-Mounted Beam Construction

The implementation shown in Fig. 3, with an offset, was used in this work. The beam is attached directly to the motor [3, 4]. This eliminates problems caused by drive train slippage, such as loss of reference, as experienced by Ito, which were solved by using a direct-mount construction [3].

Fig. 3: Motor-Mounted Beam

B. Sensor Selection

Many options are available to monitor beam angle and ball position. A few of the more common choices are reviewed, but the list is not intended to be exhaustive.

1) Beam Angle Sensor

A potentiometer can be attached to the beam shaft [2] or beam actuator [4] for beam angle measurement. Also, an accelerometer configured to measure the gravitational acceleration component, proportional to the sine of the beam angle [3]. In this work, an angular encoder was mounted on the motor shaft which allowed direct angle measurement [2].

2) Ball Position Sensor

Finding a reliable sensor that offers economic and high resolution, noise free measurement presents difficulty.

In [2], several versions of linear potentiometers based on a conductive ball and adjacent rails were tested. In this method, one rail conducts a constant current producing a linear voltage distribution along the rail; the other rail's voltage is monitored to determine the ball position. As the

Manuscript received September 22, 2010.

J. Wieneke is a Mechanical Engineer at Intelligrated, Mason OH 45040 (email: jacob.wieneke@intelligrated.com).

W. N. White is with the Mechanical and Nuclear Engineering Department, Kansas State University, Manhattan, KS 66506 USA (phone: 785-532-2615, fax: 785-532-7057, e-mail: wnw@ksu.edu).

ball rolls on the rails, the sensed voltage determines the ball location. The method was used in several ball-and-beam projects [2, 3, 4, 5]. The sensor's major benefit is low cost [5]. A downfall is the noise produced by the ball-rail contact and possible signal loss due to rail pits and irregularities [2, 3]. Friction could be introduced at the ball contact point, a disadvantage shown in the second option shown in Fig. 4.

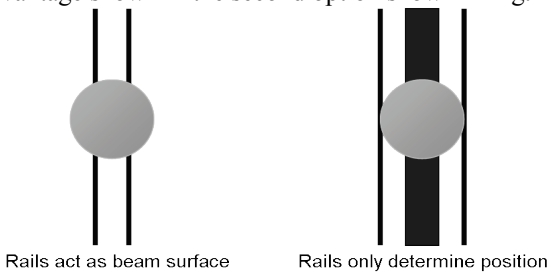

Fig. 4: Conductive rail configurations

Infrared range (IR) finders are an alternative as mentioned in [5]. This possibility was explored when an IR sensor was tested in [3]. These sensors are inherently nonlinear and it was concluded in [3] that systems using this type of sensor would require a range of gains. An IR benefit is the non-contact sensing. Drawbacks are their limited operating range and lack of precision when detecting a spherical object.

Laser range finders are another non-contact method. However, the available commercial units are either too costly or have too limited a range to be useful.

A final sensor alternative is an ultrasonic transducer [5]. In [4], these devices were tested and discarded because of range limitations. Similar to IR sensors, ultrasonic sensors offer non-contact sensing. Disadvantages include limited ranges (depending on sensor and configuration) and cost. An ultrasonic sensor was selected in this work because it could determine the ball position over the beam length.

II. Specific Construction

The ball-and-beam construction is described here. The beam materials and design are described as are the choice of sensors, motor, amplifier, ball, and control hardware.

A. Beam Construction

The beam must be lightweight, allow roll without slip, and able to support the ultrasonic sensors. Because of weight requirements, the beam material was aluminum. Two extrusion options were considered; angled aluminum was selected instead of channel as it used less material and offered a rolling surface that 'cradled' the ball.

Sensor brackets were designed and machined from aluminum blocks. The brackets point the sensors down the beam length and offer protection from the ball striking the sensor. The beam center is attached to a milled aluminum block with a press-fit shaft coupled to the motor. Fig. 5 illustrates the offset between the ball rolling surface and the rotation center.

B. Ball Sensor

The linear potentiometers require a conductive ball and involve sliding friction. A non-contact position sensor overcomes these shortfalls. The ultrasonic transducer offers accurate position measurement and eliminates the need of an electrically conductive ball, allowing a wider ball selection. After researching possible infrared and laser optical sensors, it was found that commercially available sensors measuring range were not well suited for the beam length. The Senix ToughSonic [7] ultrasonic sensors were capable of detecting various ball sizes over the required distance with a limitation that objects closer than four inches cannot be detected. The sensor selected was a Senix TSPC-30S1-232. It is configured using a PC with the SenixVIEW software so the analog 0-10 volt output is scaled to represent the desired range.

One consideration for acoustic sensors at opposing beam ends is that they may receive ultrasonic waves from each other, causing inaccurate measurements. Another is their ability to accurately determine the ball's position over the beam length. These issues are discussed in a later section.

C. Motor and Amplifier

Both the motor and amp were determined by equipment availability. The motor is a Reliance Electric brushless DC motor model BDC-T330-BVL. The motor has a Danaher Industrial Controls optical encoder model M20250011001 on the rear shaft for angular position measurement. Connected to the motor is an Advanced Motion Controls brushless PWM servo amplifier model CBE25ACB. This amplifier allows current control of the motor, supplying a current proportional to the input voltage. The amp has a built-in rectifier and connects to AC outlets [8].

The motor is directly coupled to the beam for actuation. This allows angle determination from the motor encoder.

D. Ball

A ping-pong ball was first chosen due to low inertia and availability. However, its small size made it difficult for the ultrasonic sensor to detect. A croquet ball and a toy foam ball were both tried, but neither was sufficiently smooth to facilitate easy rolling. Finally, a standard racquetball was selected. The racquetball is an attractive choice due to its availability, low inertia and mass, cost, and size.

E. Controller Hardware

The controller was selected based on compatibility and availability. Due to a recent lab renovation, real-time desktop PCs were available running National Instruments (NI) LabVIEW Real Time with NI PCIe-6361 X-series DAQs already installed. The hardware provided two crucial tools for the controller, communication and computation.

III. System Model

To develop a ball-and-beam controller, a state space system model was developed. The system model served to specify which model parameters needed to be identified.

A. System Diagram

Fig. 5 shows the free body diagram developed for dynamic model determination. One notable feature of the system is the offset distance between the beam point of

rotation and the surface the ball rolls on; other systems researched had the two points coincident. It is important to note the difference between R_o and R_{ball}; R_{ball} is the radius of the ball and R_o is the distance from the ball's center to the surface it rolls on. The dynamic model is described in [9].

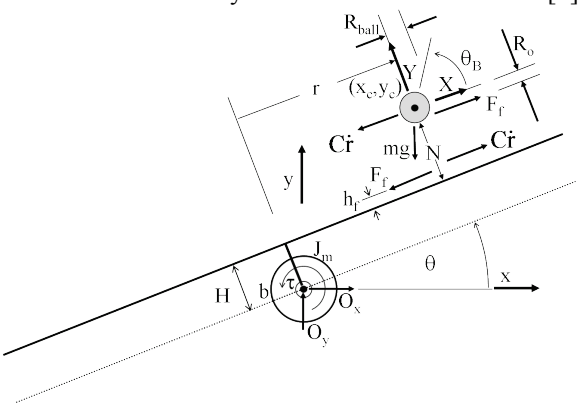

Fig. 5 Ball-and-Beam Free Body Diagram

B. Dynamic Equations

The dynamic equations are found through Newton-Euler and Lagrangian analysis. The same result was reached through both methods.

In the Lagrangian analysis, the kinetic energy is

$$T = \frac{\dot{\theta}^2}{2}\left(\bar{I} + m_b H^2 + J_m\right) + \frac{J_B}{2}\left(\dot{\theta} - \frac{\dot{r}}{R_o}\right)^2 + \frac{m}{2}\left(\left(\dot{r} - \dot{\theta}\left(R_o + H + h_f\right)\right)^2 + r_2\dot{\theta}^2\right) \quad (1)$$

where H, R_o, r, and h_f are shown in Fig. 5, $\bar{I}$ is the inertia of the beam assembly about its mass center, m_b is the mass of the beam, m is the mass of the ball, and J_m is the inertia of the motor shaft. The potential energy is

$$V = mg\left(r\sin(\theta) + \left(H + h_f + R_o\right)\cos(\theta)\right). \quad (2)$$

The Lagrangian is given by

$$L = T - V. \quad (3)$$

From the analysis, the equations of motion are found to be

$$\begin{bmatrix} \bar{I} + m_b \cdot H^2 + J_m + m \cdot R_o^2 + 2\cdot(H+h_f)\cdot m \cdot R_o + m\cdot(H+h_f)^2 + m\cdot r^2 + J_B & -\frac{J_B}{R_o} - m\cdot R_o - (H+h_f)\cdot m \\ -\frac{J_B}{R_o} - m\cdot R_o - (H+h_f)\cdot m & m + \frac{J_B}{R_o^2} \end{bmatrix} \begin{bmatrix} \ddot{\theta} \\ \ddot{r} \end{bmatrix}$$

$$+ \begin{bmatrix} b + 2\cdot m\cdot r\cdot\dot{r} & 0 \\ -m\cdot r\cdot\dot{\theta} & C \end{bmatrix} \begin{bmatrix} \dot{\theta} \\ \dot{r} \end{bmatrix} + \begin{bmatrix} -m\cdot g\cdot\left(-r\cos(\theta) + R_o\sin(\theta) + (H+h_f)\sin(\theta)\right) \\ m\cdot g\cdot\sin(\theta) \end{bmatrix} = \begin{bmatrix} \tau \\ 0 \end{bmatrix}. \quad (4)$$

In (4), b and C are viscous damping coefficients.

C. Parameter Identification

The dynamic model parameters were required. Some parameters could be directly measured such as the mass, diameter, and thickness of the racquetball and the coupling collar mass. This data are used to determine the inertias of both. The beam inertia (beam, cradle, sensor brackets, and sensors) came from the CAD software SolidWorks.

Other parameters were more difficult to identify. These were the motor inertia, motor friction, and the amplifier voltage to current gain. The motor inertia and motor friction were determined experimentally by collecting data and forming estimates. The difficulty in obtaining the amplifier gain was increased by the noisy amp current sense channel which ideally provides a voltage proportional to output current. The motor model was changed from a current-input model to a voltage-input model, to utilize the known voltage information. The transfer function of the motor is

$$\frac{\theta(s)}{I(s)} = \frac{K_t}{J_m \cdot s^2 + b \cdot s} \quad (5)$$

where θ is the position of the motor, I is the motor input current, K_t is the motor torque constant, J_m is the motor inertia, and b is the viscous friction coefficient. Because of the difficulty encountered in obtaining a measurement of the amplifier output current, the substitution of

$$I = K_v \cdot V \quad (6)$$

was used, relating the amplifier output current to its input voltage. The constant α was defined as

$$\alpha = K_v \cdot K_t. \quad (7)$$

With this substitution, the motor model is

$$\frac{\theta(s)}{V(s)} = \frac{\alpha}{J_m \cdot s^2 + b \cdot s} = \frac{\alpha/J_m}{s^2 + b/J_m \cdot s}. \quad (8)$$

Making the motor velocity the output, (8) becomes

$$\frac{s \cdot \theta(s)}{V(s)} = \frac{\alpha/J_m}{s + b/J_m}. \quad (9)$$

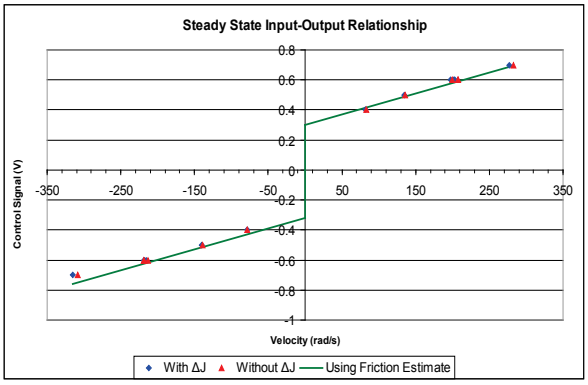

Fig. 6: Steady-state velocity -command voltage relationship

The motor inertia and friction is determined from the same experiment used to find α. First, with the motor unloaded, a known voltage range was used as system input. The resulting step response of each input was recorded to find the time constant and steady-state velocity. From (9), the time constant of the motor is $\tau_t = J_m/b$ and the relationship between steady-state velocity and input voltage is $\dot{\theta}(t) = (\alpha/b)\cdot V$, as shown in Fig. 6 together with the static friction the motor must overcome.

An exponential curve-fit of the step-response data and a linear regression applied to the velocity/voltage relationship produced the ratios J_m/b and α/b. If a motor transfer function was all that was desired, these ratios would be sufficient. However, the motor inertia and friction were needed for system simulation and controller development.

Adding a known inertia to the motor (ΔJ), performing the same tests and curve-fits as before, and finding the time constants difference, as shown in Fig. 7, an estimate of the ratio $\Delta J/b$ was had. Then b is determined from the known ΔJ. J_m and α are found from the calculated b. The collar connecting the motor to the beam assembly was used as ΔJ. Noise in Fig. 7 stems from numerical time differentiation.

IV. Acoustic Sensor Configuration

Before installing the sensors on the beam, a single sensor was purchased and tested to demonstrate that it could sense the ball position statically and dynamically. After successful tests, the apparatus was built and another sensor purchased. However, two sensors caused some measurement problems.

A. End-to-End

This configuration was intended to eliminate the dead zones immediately in front of each sensor. To accomplish this, each sensor would measure the ball's position anywhere on the beam, from its dead zone to the opposite end. Then, a switching algorithm would determine which sensor was giving a correct reading, based on measured and estimated ball positions. Given what was known about the sensors prior to testing, this configuration made the most sense, but in practice this configuration could not be implemented.

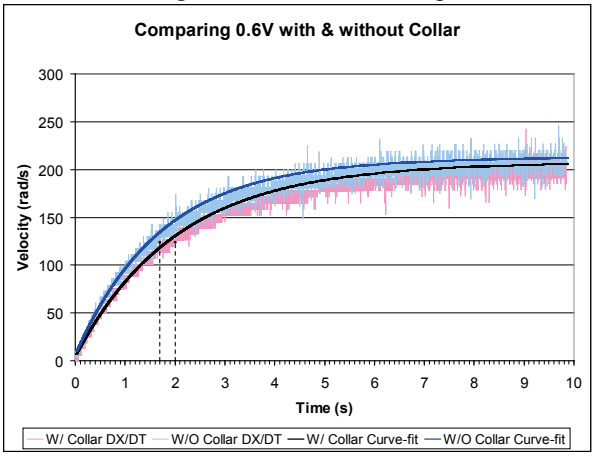

Fig. 7: Time Constant Difference and 0.6 Volt Step Responses

While the sensor specifications given in the data sheet appear correct for a larger, flat surface, they are difficult to realize when measuring a smaller, spherical surface. For the sensors to measure the ball position accurately the gains needed to be increased, which limited the range. The shorter range prevented the sensors detecting the ball at the opposite end of the beam, so the configuration needed to be changed.

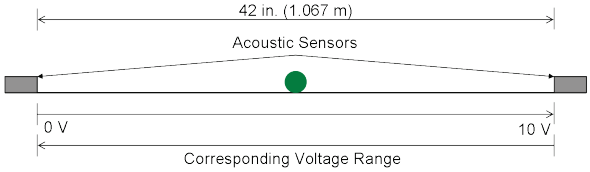

Fig. 8: End-to-End configuration

The next configuration choice was for each sensor to find the ball position on half the beam length, as the ball should not enter the sensor dead zones during normal operation.

B. End-to-Center

In this configuration each sensor measures the ball position from its dead zone to the beam center. The sensor output voltages were arranged as illustrated in Fig. 9. This arrangement allowed for adding the voltages to determine the ball's position along the beam length. However, this configuration had unexpected results.

First, with both sensors taking measurements continuously and aimed directly at each other, the ultrasonic waves interfered with the opposite sensor's measurement, as illustrated in Fig. 10. The points labeled V1 are the voltage from the first sensor, V2 is the voltage from the second sensor plus 10V to line up with the ideal linear regression, and V3 is the sensor voltage. The sensor interference is best illustrated by the points that seem coincident with a line having a negative slope. Ideally, the V1 points above 54.6 centimeters (beam center) should all be at 10 volts; similarly with the V2 points below 54.6 centimeters. Then the V3 points would all be along a single line with positive slope.

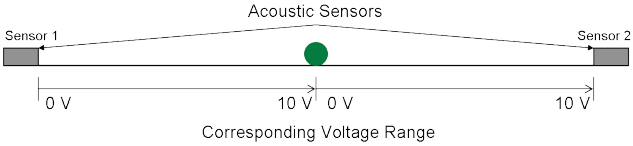

Fig. 9: End-to-Center configuration

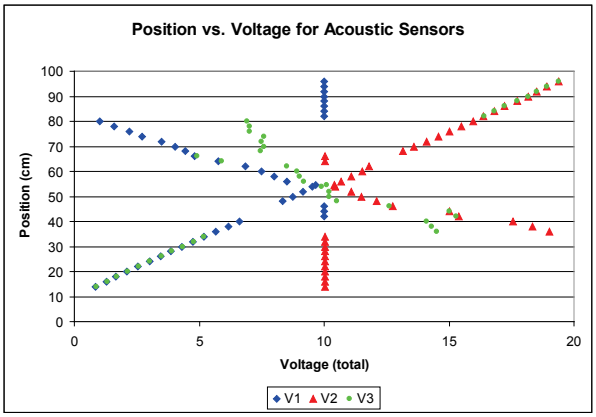

Fig. 10: Position as a Function of Sensor Voltage with Interference

This interference is not constant, so the sensors do not always provide the shown voltages; the output voltage actually alternates between the ideal and the undesired, negative slope line. As a result, it became necessary to coordinate the sensor firings. This was accomplished by establishing sensor one as a master and sensor two as a slave. The master sensor controls alternating measurements with the slave. With this change a linear fit could be developed.

It is seen in Fig. 11 that even though a linear regression can be performed on the V3 data, there are two spots where small groups of points do not match with the trend line.

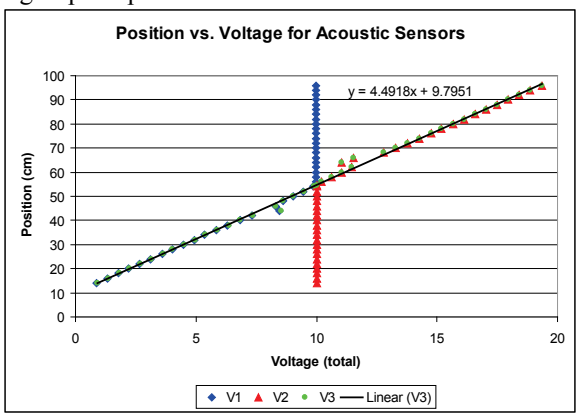

Fig. 11: Position as a function of Sensor Voltage with V3 linear fit

With the alternating sensors, interference could not have been the cause. Also, the abnormal spots created disturbances in the controller that caused instabilities. After further analysis, it was determined that these unpredictable zones were caused by the target selection; using a larger target, or a target with a non-spherical surface, resulted in reduction of these zones.

C. Overlapping

To obtain a reliable measurement of the ball position as it crossed the abnormal spots within each sensor's range, the sensor ranges were expanded to cover the unpredictable zone of the opposite sensor, as illustrated in Fig. 12. This configuration allowed accurate determination of the ball position along the full beam length (excluding sensor dead zones), and avoided requiring the controller to constantly switch sensors when the ball was in the beam center.

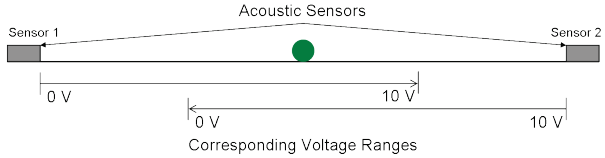

Fig. 12: Overlapping Range configuration

After implementing the overlapping configuration with the hardware, the results of Fig. 13 were obtained. There is now a linear position to voltage relationship for each sensor.

The linear regressions shown in Fig. 13 were used to create a procedure within the controller that switches between sensors, switching prior to the ball entering the unpredictable zone of a sensor, allowing for accurate ball position determination between the two sensor dead zones. The controller can maintain the use of one sensor when the ball is in the center, instead of constantly switching at that position, thus reducing conflicts within the controller.

V. Controller

This section discusses the controller for the ball-and-beam apparatus and implementation of the control algorithm.

A. Controller Selection

A pole placement, stabilizing controller was the design goal. The linearized equations of motion are

$$\begin{bmatrix} \bar{I}+m_b\cdot H^2+J_m+m\cdot R_o^2+2\cdot(H+h_f)\cdot m\cdot R_o+m\cdot(H+h_f)^2+J_B & -\frac{J_B}{R_o}-m\cdot R_o-(H+h_f)\cdot m \\ -\frac{J_B}{R_o}-m\cdot R_o-(H+h_f)\cdot m & m+\frac{J_B}{R_o^2} \end{bmatrix} \begin{bmatrix} \ddot{\theta} \\ \ddot{r} \end{bmatrix}$$
$$+\begin{bmatrix} b & 0 \\ 0 & C \end{bmatrix}\begin{bmatrix} \dot{\theta} \\ \dot{r} \end{bmatrix}+\begin{bmatrix} mg & mg\left(R_0+H+h_f\right) \\ 0 & mg \end{bmatrix}\begin{bmatrix} r \\ \theta \end{bmatrix}=\begin{bmatrix} \tau \\ 0 \end{bmatrix}. \quad (10)$$

The system poles were placed at numerous locations during simulations to find an appropriate location and the poles were chosen as [-2+2*i*, -2-2*i*, -6, -7]. The controller gains were found to be

$$K=\begin{bmatrix} 27.03 & -16.68 & 4.931 & -13.18 \end{bmatrix}. \quad (11)$$

Observer gains were calculated and the state estimator was included in the simulation and implemented in the controller.

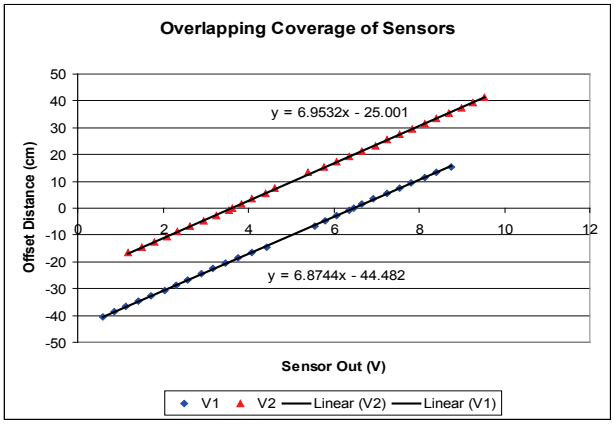

Fig. 13: Position as function of individual Sensor Voltage

B. Control Implementation

The controller was created using a PC running LabVIEW Real Time with an NI PCIe-6361 X-series multifunction data-acquisition (DAQ) board that communicates with the sensors, controller, and amplifier. The real time sample frequency is10 kilohertz which is faster than any limiting motor dynamics, so that the control loop does not adversely affect system performance.

The control program initializes all of the necessary communication channels and variables on startup. Then it launches a loop that performs sensor readings, state estimation, control calculation, control output, and data collection. The gains developed in the simulation are used in the controller implementation.

As a safety precaution and to prevent wrapping of sensor wires about the motor shaft, the control loop stops if the beam angle exceeds ±45 degrees. Otherwise, the system operates until the user stops it. This controller follows one developed at Kansas State University for controlling a motor in an undergraduate laboratory setting [10].

VI. System Performance

After constructing the system, the performance was tested. This section describes the process of improving the system model and controller so that it produced the desired control.

A. Controller Implementation

In implementing the controller, an iterative process was followed of improving simulation detail and subsequently altering the controller. The acoustic sensor updates at a rate of 100 Hz and a sample and hold was used to retain the most recent sensor output for use in the full state observer. Data sampling, observer, and control was executed at 10 kHz in hard real-time. Even with the sample time differences, the ball and beam worked well. It was noticed that a small steady state error in ball position occurred near the state space origin as illustrated in Fig. 14. As a result, the acoustic sensors were fine-tuned, further stabilizing the system by eliminating false ball positions, reducing the sensor switching when the ball centered on the beam, and providing appropriate coverage of sensor unpredictable zones. Unfortunately, a steady-state error of the position was

still present, but smaller. The steady state error led to an investigation of static friction of the motor shaft.

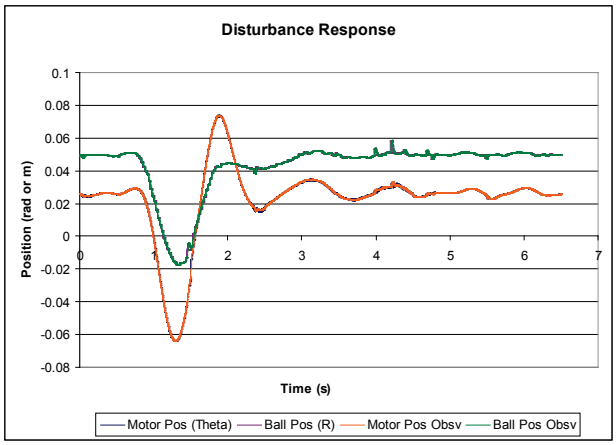

Fig. 14: Steady-state error and return after disturbance

B. *Overcoming Static Friction*

In looking at steady-state ball position error, it was seen that the ball always went to the same location and it appeared that there was not enough position error to cause the control signal to be sufficient to drive the ball to the beam center. It was assumed that this behavior was caused by static friction, or stiction, present in the motor that had not been modeled.

The controller was modified to include anti-stiction capability. Adjusting the anti-stiction limits caused a decrease in steady-state error until a very small amplitude limit cycle occurred, as illustrated in Fig. 15.

With the ball in the beam center, the disturbance rejection capability of the controller was tested. Fig. 16 shows the results. The ball was disturbed in either direction and the controller caused the beam to properly regulate the ball.

VII. Conclusion

This investigation determined the feasibility of using ultrasonic sensors for ball position measurement in a ball and beam apparatus. The selected Senix sensors were able to be configured for use in this application, as detailed in Section III. After suitable selection of parameters, the sensors worked very well, measuring the ball's position accurately so that the control was successful. As was described in Section VI, the performance improvement of adding controller anti-stiction capability was noted. The sensors performed well and it was demonstrated that acoustic sensors are a viable alternative to other methods of ball position sensing. A website for the ball-and-beam CAD drawings, images, control and data acquisition software, parts list, and video is:

http://www.mne.ksu.edu/research/laboratories/dynamic-systems-controls-laboratory-1/ball-and-beam

VIII. Acknowledgment

The authors wish to acknowledge J. Chavira, E. Martinez, N. Rauth, and V. Salazar for assisting in the development, construction, model creation, and parameter identification.

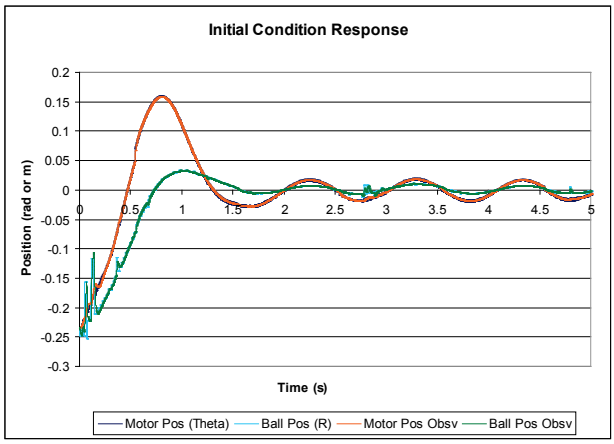

Fig. 15 Illustration of centered limit cycle

Fig. 16 Disturbance Response of final system

References

[1] Quanser Inc. "Rotary Control Challenge." www.quanser.com/english/html/challenges/fs_chall_rotary_flash.htm

[2] Rosales, Evencio A. A Ball-on-Beam Project Kit. Bachelor of Science Massachusetts Institute of Technology, 2004.

[3] Ito, Bennett T. Stabilizing the Ball on Beam System with Analog Feedback. Bachelor of Science Massachusetts Institute of Technology, 2004.

[4] Situm, Zeljko. "A Pneumatically Actuated Ball and Beam System." International Journal of Mechanical Engineering Education 36.3 (2008): 225-34.

[5] Rosales, E.A.; Ito, B.T.; Lilienkamp, K.A.; Lundberg, K.H,: "An Open-Ended Ball-Balancing Laboratory Project for Undergraduates." American Control Conference (ACC), 2004, 1314 - 1318 vol.2.

[6] Sheng, Jansen, Jay Renner and William S. Levine. "A Ball and Curved Offset Beam Experiment." American Control Conference (ACC), 2010, page(s): 402 - 408.

[7] Senix Corporation. "ToughSonic TSPC Series." Senix Corporation. www.senix.com/family_tspc.htm

[8] Advanced Motion Controls. "Analog Servo Drive10/29/2009. www.a-m-c.com/download/datasheet/be25a20ac.pdf

[9] Wieneke, Jacob, "A Feasibility Assessment of Using Ultrasonic Sensor Position Feedback for a Ball-and-Beam Apparatus," MS Thesis in Mechanical Engineeirng, Kansas State University, 2010.

[10] Wieneke, Jacob; Schinstock, Dale; White, Warren N.; Hu, Guoqiang; "Redesign of an Undergraduate Controls Laboratory with an Eye Toward Accommodating Future Upgrades." American Control Conference (ACC), 2010, 384 - 389.